Phase Diagrams for Ceramists
1975 Supplement

Ernest M. Levin and

Howard F. McMurdie
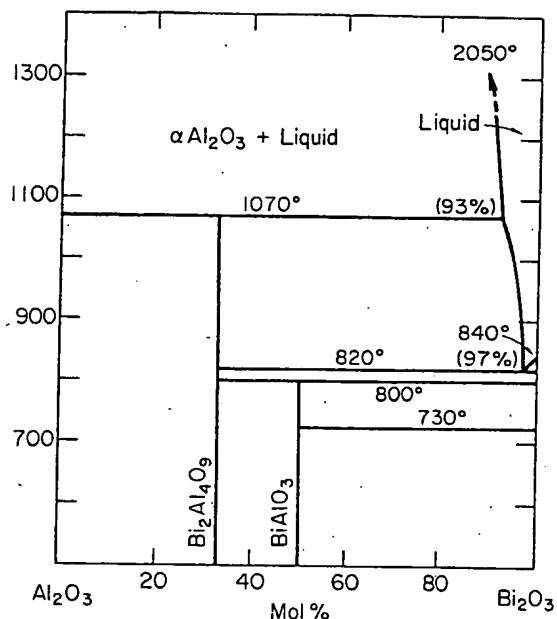
Compiled at the National Bureau of Standards

Margie K. Reser, *Editor*

Price $35

$Al_2O_3-Bi_2O_3$

FIG. 4365.—System $Al_2O_3-Bi_2O_3$.
E. I. Speranskaya, V. M. Skorikov, G. M. Safronov, and E. N. Gaidukov, *Izv. Akad. Nauk SSSR, Neorg. Mater.*, **6** [7] 1364 (1970); *Inorg. Mater. (USSR)*, **6** [7] 1201 (1970).

About 15 mixtures of Bi_2O_3 (cp) and Al_2O_3 (analytical reagent) were annealed at 780° in Pt crucibles and studied by DTA. A compound of composition $15Bi_2O_3 \cdot Al_2O_3$ (Fig. 327), identified previously by high-temperature X-ray diffractometry, was not verified, and its existence as a stable compound remains in question. At high concentrations of Al_2O_3, the system is qualitatively similar to the $Fe_2O_3-Bi_2O_3$ system (Fig. 2357).
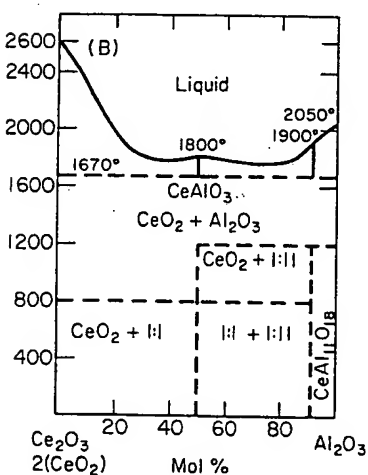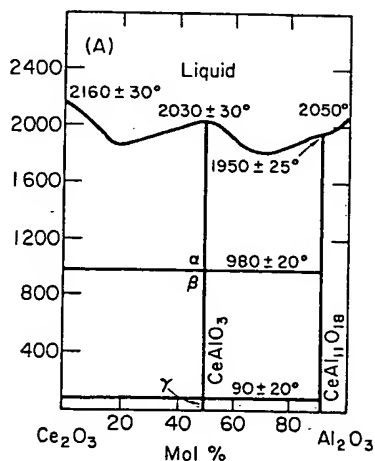
$Al_2O_3-Ce_2O_3$

FIG. 4366.—System $Ce_2O_3-Al_2O_3$ (*A*) in H_2 and (*B*) in air (pseudobinary). Under reducing conditions (*A*), Ce is trivalent from room temperature to melting. When heated in air, $CeAlO_3$ and $Ce_2O_3 \cdot 11Al_2O_3$ formed by quenching from high temperatures start to decompose at 800° and 1200°, respectively, as shown by dashed lines in (*B*).
A. I. Leonov, A. V. Andreeva, V. E. Shvaiko-Shvaikovskii, and E. K. Keler, *Izv. Akad. Nauk SSSR, Neorg. Mater.*, **2** [3] 517 (1966); *Inorg. Mater. (USSR)*, **2** [3] 446 (1966).

Methods of investigation under controlled O_2 pressure are outlined in Refs. 1 and 2. The composition of Ce_2O_3 at the mp in H_2 (2160°) was determined by weight gain during oxidation. Friedrich and Sittig[3] reported an mp in N_2 of 1692°, but the possible formation of CeN makes the value unreliable. At 1670°, $Ce^{4+} \rightarrow Ce^{3+}$ according to the reversible reactions $2CeO_2 + Al_2O_3 \rightleftharpoons 2CeAlO_3 + \frac{1}{2}O_2$ and $2CeO_2 + 11Al_2O_3 \rightarrow Ce_2O_3 \cdot 11Al_2O_3 + \frac{1}{2}O_2$. Under a vacuum of 10^{-5} mm Hg, $CeAlO_3$ begins to form at 1200°. $CeAlO_3$ has the perovskite-type structure (unit-cell and optical data given). In H_2 it exhibited 2 reversible polymorphic transformations. The compound $Ce_2O_3 \cdot 11Al_2O_3$ is identical with $La_2O_3 \cdot 11Al_2O_3$ (Fig. 2340), showing the βAl_2O_3-type structure. Electrical-property data are given. See also Fig. 4394 for a study of the companion system $Ce_2O_3-Cr_2O_3$.

1. A. I. Leonov and E. K. Keler, *Izv. Akad. Nauk SSSR, Otd. Khim. Nauk*, **1962**, No. 11, p. 1905.
2. A. I. Leonov, *ibid.*, **1963**, No. 1, p. 8.
3. E. Friedrich and L. Sittig, *Z. Anorg. Allg. Chem.*, **145**, 127 (1925).

$Al_2O_3-Eu_2O_3$
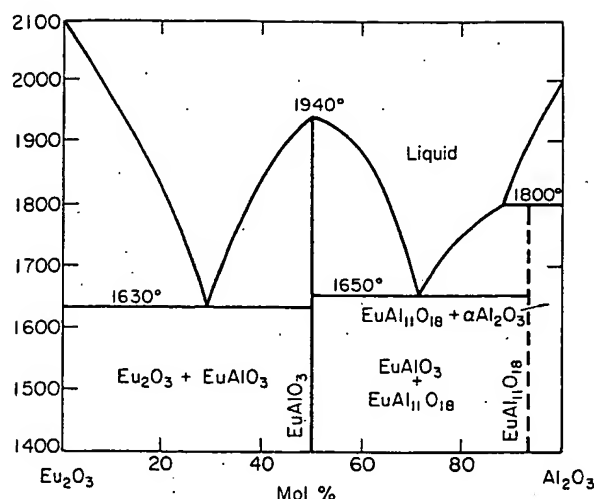
Eu_2O_3, 99.8% pure, and Al_2O_3, obtained by roasting $Al(NO_3)_3$ (analytically pure) at 600° for 2 to 3 h, were dissolved in HNO_3 (1:5), evaporated to crystallization, roasted in air at 700° to 800° until the N oxides disappeared, and pressed into pellets. Mixtures were formulated in 1 to 5% intervals and heated at 600°, 800°, 1000°, 1200°, 1250°, 1400°, 1600°, and 1700°. Melting values (averages of 5 to 7 runs) were determined in spectrally pure Ar (0.005% O_2) in a miniature furnace with a W heater by a noncontact method of heating and measured with an optical pyrometer to an accuracy of ±50°. Samples were cooled in a gas medium at 100° to 150°/s. X-ray diffraction, chemical, and metallographic methods of analysis were used.
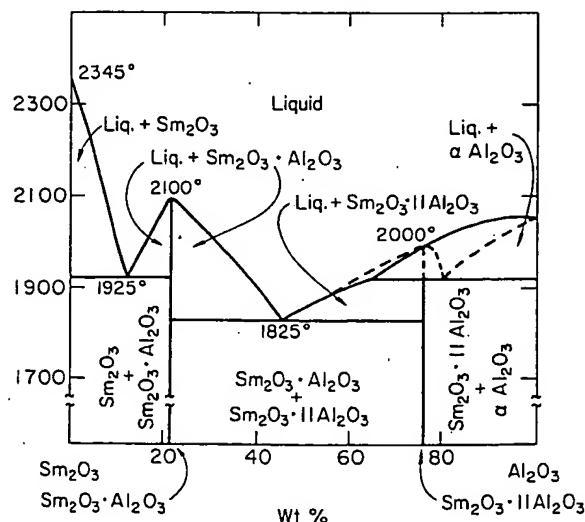
The compound $Eu_2O_3 \cdot 11Al_2O_3$ was detected by X-ray diffraction (unindexed powder pattern given); however, it could not be obtained in pure form and was found mixed with αAl_2O_3 and $EuAlO_3$. Excluding the questionable 1:11 compound, the subsolidus is in agreement with Fig. 312. The mp of Al_2O_3 shown at 2000° is 54° below the recommended value of 2054° ± 6° (International Practical Temperature Scale, 1968).[1] Density, microhardness, and some solubility data are listed for Eu_2O_3 and $EuAlO_3$.

1. S. J. Schneider, *Pure Appl. Chem.*, **21** [1] 117 (1970).

$Al_2O_3-Gd_2O_3$
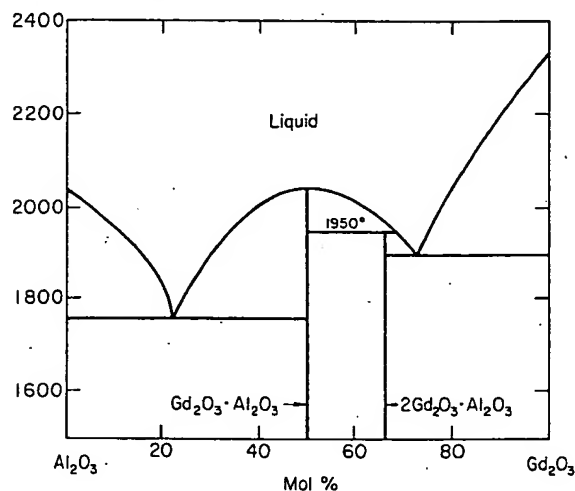
Fourteen starting mixtures, prepared by coprecipitation of Al and Gd hydroxides, were calcined at 880° (55 h), 930° (1 h), and 1380° (1 h) and analyzed by X-ray, microscopic, and microhardness techniques. Thermal analysis methods established melting points. Compounds were also verified by examination of fused samples annealed at 1700°. An unindexed X-ray pattern of the 2:1 compound is given. The diagram agrees with the subsolidus data of Fig. 312.

$Al_2O_3-Sm_2O_3$

Experimental details are outlined in the commentary to Fig. 4371. This and other work reported on the system (see Fig. 312 and reference cited for Fig. 4368) are in conflict regarding the existence of the various compounds. All agree on the occurrence of the 1:1 phase; however, the acceptance of the 2:1 and 1:11 compounds depends on further verification.
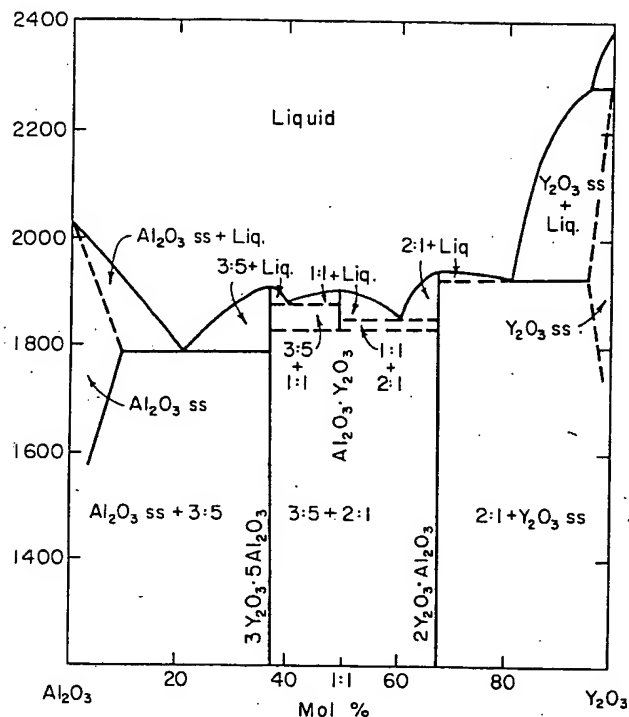
$Al_2O_3-Y_2O_3$

$Al_2O_3-Yb_2O_3$

FIG. 4371.—System $Yb_2O_3-Al_2O_3$. Compound ratios are given in the order $Yb_2O_3:Al_2O_3$.

I. A. Bondar and N. A. Toropov, *Izv. Akad. Nauk SSSR, Ser. Khim.*, 1966, No. 2, p. 213; *Bull. Acad. Sci. USSR, Div. Chem. Sci.*, 1966, No. 2, p. 195.

FIG. 4370.—System $Al_2O_3-Y_2O_3$, tentative. $3Y_2O_3 \cdot 5Al_2O_3$ (3:5) = garnet structure type; $Y_2O_3 \cdot Al_2O_3$ (1:1) = perovskite; $2Y_2O_3 \cdot Al_2O_3$ (2:1) = monoclinic symmetry.

T. Noguchi and M. Mizuno, *Kogyo Kogaku Zasshi*, **70** [6] 839 (1967).

Twenty-four samples were studied by solar heating and rapid-cooling curves. Liquidus temperatures were measured by a brightness pyrometer at 0.65 μm. Fused samples were examined by X-ray diffraction. See Fig. 4259 for general experimental details. Previous work on this system is shown in Figs. 311, 312, and 2344. Noguchi and Mizuno, contrary to Fig. 311 but in agreement with Figs. 312 and 2344, report a 1:1 compound. Their work disagrees, however, with Fig. 2344 in suggesting that the 1:1 compound melts congruently. Indexed X-ray patterns of this compound here and in Ref. 1 seem to confirm that it exists, at least metastably. The methods used in the present work are probably not sensitive enough to prove congruency of melting. Indexed X-ray patterns of the 3 binary compounds are given.

1. R. S. Roth, *J. Res. Nat. Bur. Stand.*, **58** [2] 75 (1957).

Samples were prepared by annealing mixtures of 99.9 to 99.95% Yb_2O_3 and 99.9% Al_2O_3, or, in some instances, the coprecipitated hydroxides. Phases present in annealed or quenched samples were identified by techniques including X-ray diffraction and microscopy and by density and microhardness measurements. Figure 312 and the present work agree with the exception of the instability of the 2:1 compound below 1675°. A table of properties (structure types, optical data, mp, hardness, density) is given for the compounds in this and similar rare-earth systems (La_2O_3, Sm_2O_3, Tb_2O_3, and Y_2O_3).
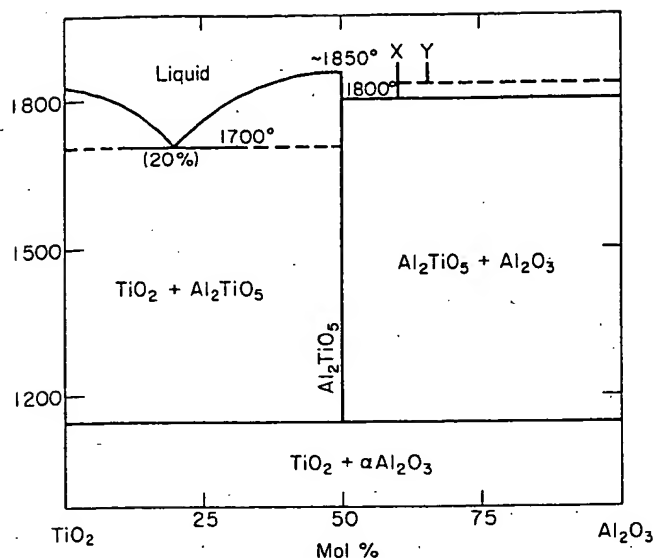
Al$_2$O$_3$–TiO$_2$

The principal objective of the work was to study compounds formed in systems of TiO$_2$ with R$_2$O$_3$ metal oxides, such as R$_2$TiO$_5$ with the pseudobrookite structure type. Al$_2$TiO$_5$ was prepared by calcination above 1200° of coprecipitated hydrates obtained by the reaction of NH$_3$ on mixtures of TiCl$_4$ and AlCl$_3$ solutions.

The maximum solid solubility of TiO$_2$ in Al$_2$O$_3$ is ≈0.30%; the solubility of Al$_2$O$_3$ in TiO$_2$ is nil. With the addition of Fe$_2$O$_3$ to Al$_2$TiO$_5$, Fe$_x$Al$_{2-x}$TiO$_5$ is formed, which is stable at room temperature.[1]

Two new phases, not shown in Fig. 316, were reported, with compositions between 60 and 66% Al$_2$O$_3$ and the approximate stability range between 1800° and 1900° (X and Y of Fig. 4376). In a more detailed study, Goldberg[1] compared different TiO$_2$–R$_2$O$_3$ systems and discussed new phases formed in the Al$_2$O$_3$–TiO$_2$ system during reduction by H$_2$ and C at high temperatures. Microhardness values of various Al$_2$O$_3$ solid solutions are discussed.

1. D. Goldberg, *Rev. Int. Hautes Temp. Refract.*, 5 [3] 181 (1968).

Al$_2$O$_3$–ZrO$_2$
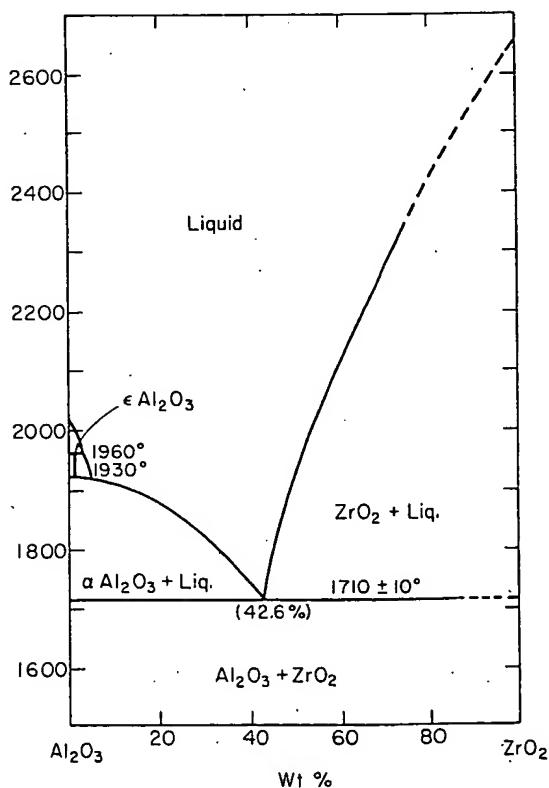
Starting materials were reagent-grade ZrO$_2$ and Al$_2$O$_3$ (purity 99.88%) which had been heated to 1350° for 15 h. Mixtures were formulated at 5% intervals and additionally at 0.2% intervals in the regions 55 to 59% Al$_2$O$_3$ and 95 to 100% Al$_2$O$_3$. Ground mixtures with < 70 wt% ZrO$_2$ were melted in W crucibles in a vacuum furnace. Mixtures with > 70 wt% ZrO$_2$ were heated in an electric arc furnace. The melting temperatures were measured with a calibrated optical pyrometer, and observations were made on 2 series of compositions, one for heating and one for cooling. The composition Al$_2$O$_3$:ZrO$_2$ (99:1 wt%), when fused in the arc furnace and quenched in H$_2$O, yielded a new phase, εAl$_2$O$_3$. The phase was indexed on a hexagonal unit cell but with several low-angle peaks unaccounted for. The new phase was verified by high-temperature X-ray diffractometry, using an Ir strip furnace and optical pyrometry. However, the high-temperature X-ray pattern reproduced is not convincing. The solubility of Al$_2$O$_3$ in ZrO$_2$ was not studied because of the more general problem of the stabilization of tetragonal ZrO$_2$. For a version of the system in an Ar atmosphere, see Fig. 4378. The polymorphism of pure ZrO$_2$ is shown in Fig. 4259.
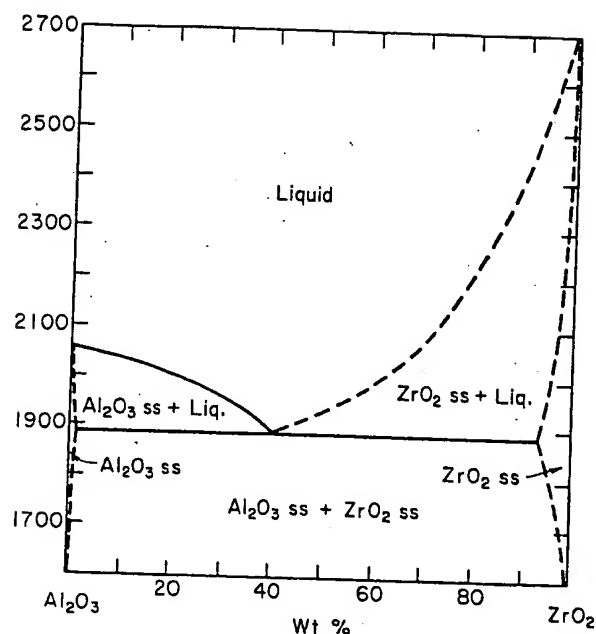
Al_2O_3–ZrO_2 (concl.)

FIG. 4378.—System Al_2O_3–ZrO_2 in Ar.
A. M. Alper, p. 339 in Science of Ceramics, Vol. 3. Edited by G. H. Stewart. Academic Press Inc. (London) Ltd., 1967.

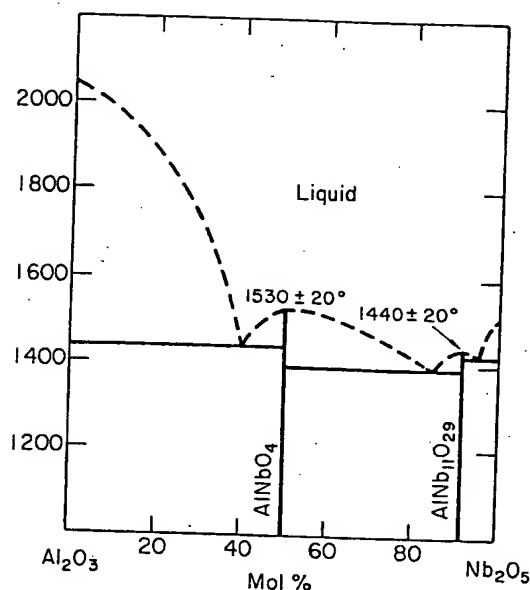Experiments were conducted in an induction furnace, with setter materials of the same compositions as the mixtures being heated. About 16 samples were melted in an Ar atmosphere, and temperature was measured with an optical pyrometer. According to Ref. 1, < 1% ZrO_2 goes into solid solution in αAl_2O_3, and up to ≈7% Al_2O_3 can form a solid solution with ZrO_2. The distribution of phases obtained was found to be related to the phase diagram and was dependent on composition and cooling rate. See Fig. 4377 for an alternate version showing a new "ϵAl_2O_3" phase. The phases of pure ZrO_2 are discussed in the commentary to Fig. 4259.

1. A. M. Alper, R. N. McNally, and R. C. Doman, *Amer. Ceram. Soc. Bull.*, **43** [9] 643 (1964) (abstract).

Al_2O_3–Nb_2O_5

FIG. 4379.—System Al_2O_3–Nb_2O_5, proposed.
E. N. Isuprova, N. A. Godina, and E. K. Keler, *Izv. Akad. Nauk SSSR, Neorg. Mater.*, **6** [8] 1465 (1970); *Inorg. Mater. (USSR)*, **6** [8] 1292 (1970).

Specimens at ≤ 5 mol% intervals were obtained by mixing γAl_2O_3 and Nb_2O_5 and coprecipitating them with NH_4OH or by mixing an aqueous solution of $Al(NO_3)_3$ with an alcoholic solution of $NbCl_5$. The roasting temperature was 600° to 1600°. Reactions were studied by X-ray powder diffraction (schematic line diagrams shown), thermal analysis of coprecipitated compositions (heating curves shown), and by chemical analysis.

Previous work indicated a number of Nb_2O_5-rich compounds, e.g. $Al_2O_3 \cdot 9Nb_2O_5$ and $Al_2O_3 \cdot 25Nb_2O_5$ (in Fig. 2349), and $Al_2O_3 \cdot 49Nb_2O_5$.[1] These compounds were not found in heat treatments below the solidus for up to 96 h. Only $AlNb_{11}O_{29}$ was detected, with an X-ray pattern apparently isostructural with $Ti_2Nb_{10}O_{29}$ (general formula $B_{12}O_{29}$).[2] It should be noted, however, that unindexed X-ray powder patterns are insufficient to characterize homologous series-type compounds, which have been predicted.[3,4]

Six compositions between 25 and 91.7 mol% Ta_2O_5 were investigated in the system Al_2O_3–Ta_2O_5, up to 1600°. Only one compound, $AlTaO_4$, was found.

1. V. K. Trunov, L. M. Kovba, and Z. Ya. Pol'shchikova, *Zh. Neorg. Khim.*, **13** [6] 1494 (1968).
2. A. D. Wadsley, *Acta Crystallogr.*, **14**, 664 (1961).
3. R. S. Roth and A. D. Wadsley, *Naturwissenschaften*, **51** [11] 262 (1964).
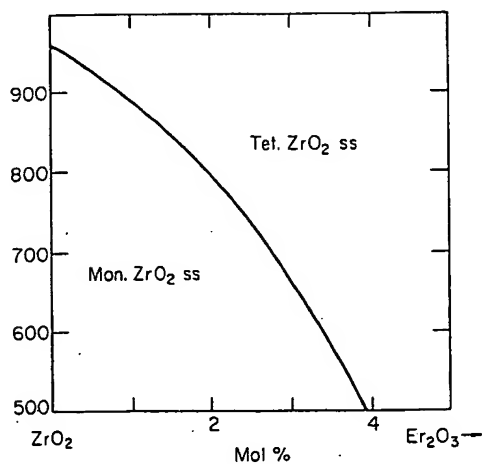4. R. S. Roth and A. D. Wadsley, *Acta Crystallogr.*, **19** [1] 26 (1965).

Er$_2$O$_3$-ZrO$_2$

FIG. 4404.—System ZrO$_2$-Er$_2$O$_3$, showing monoclinic (*Mon.*) to tetragonal (*Tet.*) inversion of ZrO$_2$.

R. K. Stewart and O. Hunter, Jr., *J. Amer. Ceram. Soc.*, 53 [7] 422 (1970).

FIG. 4405.—System ZrO$_2$-Er$_2$O$_3$ above 2000°; *bcc* = body-centered cubic, *fcc* = face-centered cubic, *Hex* = hexagonal, *Tet* = tetragonal.

A. Rouanet, *C. R. Acad. Sci., Ser. C,* 267 [23] 1582 (1968).

Starting materials were 99.97% Er$_2$O$_3$ (supplied by the Ames Laboratory of the U.S. Atomic Energy Commission) and ZrO$_2$ from 2 sources, one containing 0.49% impurities + 0.045% Hf and the other 0.14% impurities + 1.5% Hf. Powders were mixed with H$_2$O, dried, and pressed into rectangular bars at 50,000 psi. Specimens were fired at 1950°–2000° for 2 h in a reducing atmosphere, heated in air at 1250° for 12 h, and cooled to room temperature at 40° to 70°/h.

Thermal expansion curves were obtained from room temperature to 1200° using a linear variable differential transformer. Phases were identified by Debye-Scherrer X-ray diffraction techniques. Boundary data on the transformation curve (5 points) were taken from linear expansion curves at the points indicating the start of the transformation on cooling. A 2-phase region required by the phase rule is not indicated. At 6.7 to 13.5% Er$_2$O$_3$ (not shown on diagram), the material had a single-phase fluorite-type structure (cubic unit-cell dimensions given). Rouanet[1] reported the dimensions of the fluorite-type cell up to 25.0% Er$_2$O$_3$ additions.

1. A. Rouanet, *C. R. Acad. Sci., Ser. C,* 267 [23] 1581 (1968).

Twenty-two compositions, evenly distributed, were studied by thermal analysis for the determination of the liquidus curve and the solidus on the Er$_2$O$_3$-rich side. Seventeen compositions, all on the Er$_2$O$_3$-rich side, were studied by high-temperature X-ray diffraction to determine the subsolidus relations.

An interesting feature of this system is the continuous series of solid solutions varying from fcc on the ZrO$_2$-rich side to a bcc superstructure on the Er$_2$O$_3$-rich side. The line of demarcation is shown at that composition where the superstructure lines were first apparent by X-ray diffraction. A graph of cell size vs composition at room temperature is given for this series. There is some question as to the exact location of the subsolidus lines, since they are inconsistent as shown.

For similar studies on the ZrO$_2$-Y$_2$O$_3$ and ZrO$_2$-Yb$_2$O$_3$ systems see Figs. 4437 and 4440. The polymorphism of ZrO$_2$ is discussed with Fig. 4259.

Gd_2O_3–UO_2
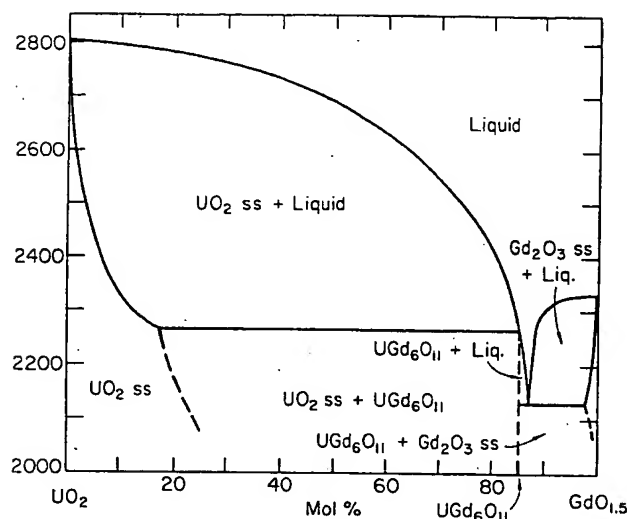
FIG. 4416.—System UO_2–$GdO_{1.5}$ in He, proposed. UGd_6O_{11} has been relocated from 75% $GdO_{1.5}$ to 85.7% $GdO_{1.5}$ to conform with the $GdO_{1.5}$ component, as agreed on in private communication with R. J. Beals. The compilers have also changed the slope of the dashed portion of the UO_2 ss boundary to be consistent with the experimental data.

R. J. Beals, J. H. Handwerk, and B. J. Wrona, *J. Amer. Ceram. Soc.*, **52** [11] 580 (1969).

Depleted UO_2 from 3 commercial sources was used. Initial O/U ratios were between 2.05 and 2.08, with principal impurities Al, Si, Fe, and Ni (typical analysis given). The Gd_2O_3 was $\geq$ 99.9% pure, with principal impurities of Si, Ca, and Fe. About 13 mixtures, well distributed, were wet-mixed, vacuum-dried, granulated, pressed into pellets, and sintered at 1700° for 4 h in purified H_2. Sintered compositions were verified by wet chemical analysis. X-ray powder diffraction analysis was used to determine lattice parameters of the solid solutions formed at 1700° (table given).

Solidus and liquidus temperatures were determined in an atmosphere of flowing high-purity He on fragments of the sintered material heated in the apex of a tungsten V-shaped wedge. The wedge acted as both holder and heater. Temperature was measured by sighting a calibrated disappearing-filament optical pyrometer into the wedge. Temperature readings were calibrated against the mp's of Ni, Fe, Pt, Rh, Ir, and Mo. The solidus was taken to be the temperature at which sharp corners of the specimen became rounded; the liquidus was taken to be the temperature at which molten material filled the apex. At least 5 determinations of solidus and liquidus values were made for each composition.

The spread in solidus temperature values for a single composition was as much as 230° and for liquidus data nearly 200°. The compound UGd_6O_{11}, made by Aitken *et al.*[1] by reaction in air at 1550° for 84 h, was not found in the present work but is shown on the diagram. A plot of a_0 of fcc UO_2 ss vs composition at 1700° indicated 60% $GdO_{1.5}$ in solid solution with UO_2 at this temperature. Weight losses, determined by thermogravimetric analysis in dry flowing H_2 at 2350°, 2500°, 2650°, and 2850° for a number of UO_2–rare-earth-oxide systems were studied for the

stabilization of UO_2. This system requires additional studies, particularly in the subsolidus region above 1700°.

1. E. A. Aitken, S. F. Bartram, and E. F. Juenke, *Inorg. Chem.*, **3** [7] 949 (1964).

Gd_2O_3–ZrO_2
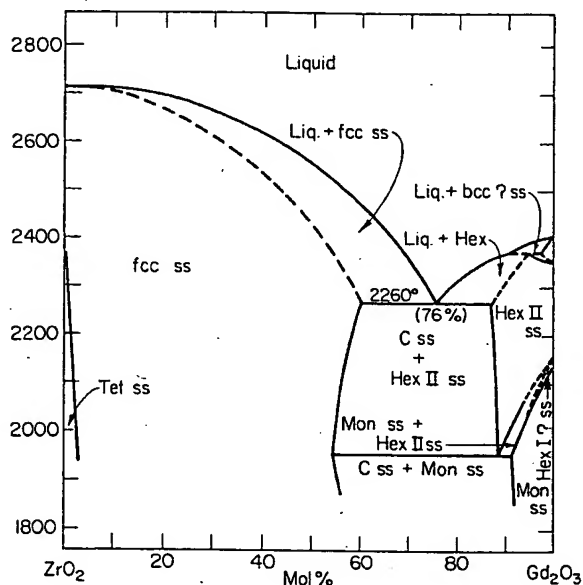
FIG. 4417.—System ZrO_2–Gd_2O_3 at high temperature; bcc = body-centered cubic, fcc = face-centered cubic, Hex = hexagonal, Mon = monoclinic, Tet = tetragonal; C ss = cubic solid solution, possibly bcc.

A. Rouanet and M. Foex, *C. R. Acad. Sci.*, Ser. C, **267** [15] 875 (1968).

The liquidus curve was derived from cooling curves obtained by the solidification of 20 compositions melted in a solar furnace. Phase relations in the region 65 to 95% Gd_2O_3 were observed at temperature by X-ray diffraction.

The diagram disagrees with previous work on the polymorphism of Gd_2O_3 regarding the presence of the hexagonal and high-temperature bcc phases (see Figs. 2369, 4255). The high-temperature X-ray method was not sensitive enough to reveal superstructure lines, which distinguish the C-type rare earth (low-temperature bcc) from a high-temperature fcc phase, as discussed in the commentary to Fig. 4433. The limit of detection of the bcc phase was 65% Gd_2O_3 at 1600° and 70% at 1750°.

On the Gd_2O_3-rich side, the diagram differs considerably from Fig. 2369. (Refer to Fig. 4433 for a brief discussion of the experimental techniques.) On the ZrO_2-rich side, Fig. 2370 shows subsolidus phase separation below 1800°. In this study, samples prepared by coprecipitation of the oxides and yielding a single phase at high temperature decomposed at 1500° into 2 solid solutions, as shown. Figure 2369 shows a pyrochlore-type ss phase, $Gd_2Zr_2O_7$, undergoing an order-disorder transformation at $\approx$1550°, a temperature well below that studied for Fig. 4417.

Nd$_2$O$_3$–ZrO$_2$

BEST AVAILABLE COPY
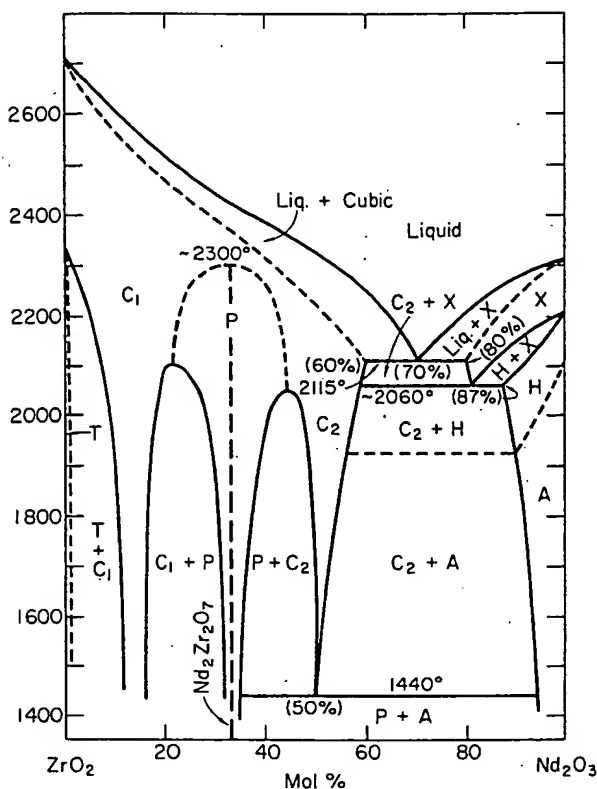
FIG. 4426.—System ZrO$_2$–Nd$_2$O$_3$. Symmetry of the solid-solution phases: *A*, hexagonal; *C*$_1$, fluorite-type cubic; *C*$_2$, Tl$_2$O$_3$-type body-centered cubic; *H*, hexagonal; *P*, cubic pyrochlore; *T*, tetragonal; *X*, probably body-centered cubic.

A. Rouanet, *C. R. Acad. Sci., Ser. C*, 270 [9] 803 (1970).

This diagram differs in details from previously reported incomplete diagrams (Figs. 350, 2382, and 2383) but resembles most closely Fig. 2382. Figure 4426 must be considered the best diagram to date because of the high-temperature X-ray study and the knowledge of the previous versions available to the experimenters. For polymorphism of ZrO$_2$, see Fig. 4259.

1. M. Foex and J. P. Traverse, *Rev. Hautes Temp. Refract.*, 3 [4] 429 (1966).

The liquidus was determined by thermal analysis of 23 uniformly distributed compositions, and the subsolidus relations were deduced from thermal analysis and by X-ray diffraction both of quenched samples and at high temperature. Further experimental details are not given.

The *X* phase could not be quenched and was difficult to study at high temperature because of high volatility of Nd$_2$O$_3$ above 2000°; consequently, its homogeneity range could not be ascertained. The *H*-to-*A* transformation between the high and low hexagonal forms, observed sharply for pure Nd$_2$O$_3$,[1] was not sharply defined in the solid solution. The eutectoid reaction at 1440° was determined by the X-ray diffraction studies at temperature. The composition Nd$_2$Zr$_2$O$_7$ does not conserve its ordered structure above ≈2300°, as indicated also by the inflection in the liquidus curve and a thermal expansion less than that for the disordered solid solutions (thermal expansion curves are shown). The 2 diphase regions *C*$_1$ + *P* and *C*$_2$ + *P* could be developed by annealing previously melted samples at 1800°. The fluorite-type ZrO$_2$ ss (*C*$_1$) was completely stabilized with a 15% addition of Nd$_2$O$_3$. The question of the reversibility of the *T* ⇌ *C*$_1$ transformation was not resolved.

Nd$_2$O$_3$–WO$_3$

FIG. 4427.—System WO$_3$–Nd$_2$O$_3$ to 1400°.

E. Ya. Rode and V. N. Karpov, *Izv. Akad. Nauk SSSR, Neorg. Mater.*, 2 [4] 683 (1966); *Inorg. Mater. (USSR)*, 2 [4] 590 (1966).

About 22 compositions between 0 and 50% Nd$_2$O$_3$ were formulated from WO$_3$ (spectrally pure) and Nd$_2$O$_3$, supplementarily purified. The construction of the diagram took into account the heating, cooling, and reheating curves of the calcined mixtures. X-ray diffraction of the compounds and mixtures confirmed the phase relations. Unindexed X-ray powder diffraction data are tabulated for the 5 compounds, and limited optical data are given for Nd$_2$(WO$_4$)$_3$, Nd$_2$W$_2$O$_9$, and Nd$_2$WO$_6$.

Nd$_2$W$_2$O$_9$, Nd$_4$WO$_9$, and Nd$_6$WO$_{12}$ have not been reported previously. Prolonged heating of Nd$_2$(WO$_4$)$_3$ at 1350° to 1400° caused a loss of WO$_3$. The mp of Nd$_2$WO$_6$ is after Ref. 1.

1. H. J. Borchardt, *J. Chem. Phys.*, 39 [3] 504 (1963).

Sc_2O_3–ZrO_2
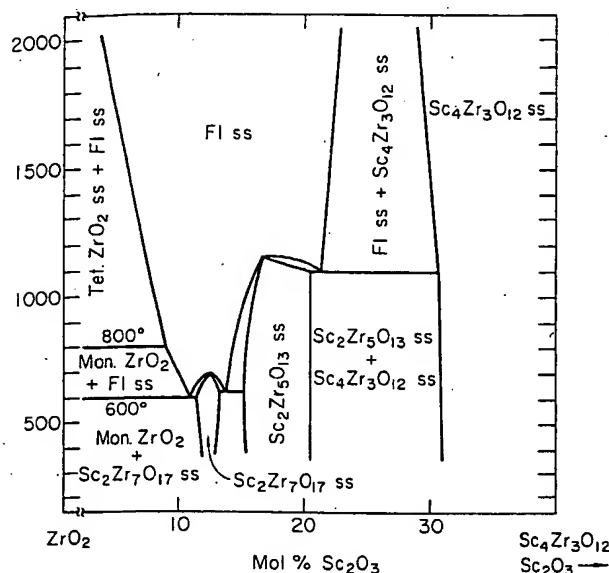
FIG. 4430.—System ZrO_2–$Sc_4Zr_3O_{12}$, partial subsolidus. *Fl ss* = fluorite-type cubic ss; *Mon* = monoclinic; *Tet* = tetragonal. $Sc_2Zr_7O_{17}$, $Sc_2Zr_5O_{13}$, and $Sc_4Zr_3O_{12}$ show rhombohedral symmetry.

F. M. Spiridonov, L. N. Popova, and R. Ya. Popil'skii, *J. Solid-State Chem.*, 2 [3] 432 (1970).

About 17 compositions, with 14 containing < 20% Sc_2O_3, were prepared from 99.8% pure ZrO_2 and 99.8% Sc_2O_3 by precipitating scandium hydroxide from HCl solution with NH_4OH at pH 8 to 9 in a highly dispersed suspension of ZrO_2 (average particle size <1 μm). The mixtures were dehydrated, pressed into pellets, and annealed as follows, with subsequent quenching: 1200°/400 h, 1400°/125 h, 1700°/10 h, and 2000°/2 h. Final heat treatments were conducted in air up to 1700° and in a vacuum furnace with W elements at 2000°.

Subsolidus phase relations were established by (1) X-ray powder diffraction analysis of quenched specimens and at temperature; (2) DTA with a photographic recording pyrometer at heating and cooling rates of 5°/min, with an accuracy of ±10°; (3) dilatometry, with a graphite dilatometer in a W furnace at a temperature change rate of 5°/min; and (4) conductivity in air up to 1500° by the double-probe method with an ac current of 1000 Hz and a heating rate of 6° to 7°/min.

The system is characterized by phase relations at high temperatures which are completely different from those at low temperatures (600° to 1100°). The 4 solid-solution phases have been reported previously, as e.g. in Fig. 2385, where α corresponds to *Fl ss*, β to $Sc_2Zr_7O_{17}$ ss, γ to $Sc_2Zr_5O_{13}$ ss, and δ to $Sc_4Zr_3O_{12}$ ss. However, it was shown in the present work, with the aid of high-temperature X-ray diffractometry, that the γ phase is not stable to 2000° (Fig. 2385) but undergoes a rhombohedral-to-cubic transformation at ≈1100°.

The magnitude of the electrical conductivity was found to be very sensitive to structural changes (temperature-dependence curves for 11 compositions are given). The energy of activation for electrical conductivity is also given for 9 compositions between 6.0 and 40.0% Sc_2O_3. A table showing variation in unit-cell dimension with composition is presented for the cubic *Fl ss* phase at 1200°. Coefficient of thermal expansion data are given for

$Sc_2Zr_7O_{17}$ (between 20° and 1000°), $Sc_2Zr_5O_{13}$ ss (3 compositions between 20° and 1200°), and $Sc_4Zr_3O_{12}$ ss (2 compositions between 20° and 1200°).
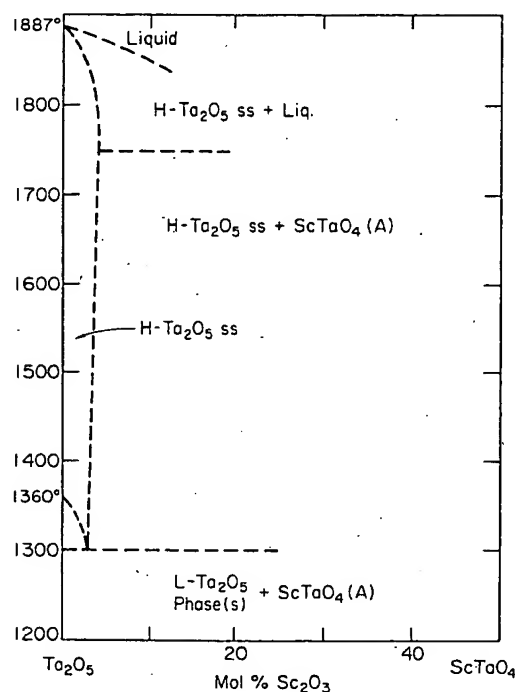
Sc_2O_3–Ta_2O_5

FIG. 4431.—System Ta_2O_5–Sc_2O_3, postulated Ta_2O_5-rich region. A = $AlNbO_4$-type structure.

R. S. Roth, J. L. Waring, and W. S. Brower, *J. Res. Nat. Bur. Stand.*, Sect. A, 74 [4] 482 (1970).

By general quantitative spectrochemical analysis, the Ta_2O_5 contained < 1% Al, Si; < 0.1% Cu, Mg; < 0.001% Ag, Ca, Mn. The Sc_2O_3 starting material was reagent grade. Four compositions containing 2, 3, 5, and 10% Sc_2O_3 were formulated by the solid-state method of mixing, pelletizing, and calcining in air at 1000° to 1200° for 10 h. After this preliminary heat treatment, portions of the ground specimens were placed in sealed Pt tubes and heated in a quenching furnace at temperatures between 1327° and 1737° for 0.5 to 72 h. The samples were quenched into H_2O and examined by X-ray diffraction powder techniques.

Insufficient data were collected to establish the exact nature of the phase diagram. No attempt was made to delineate the metastable equilibrium relations of the H-Ta_2O_5 ss phase transitions, as was done previously in the Ta_2O_5–TiO_2 system (Fig. 2403). Small crystals of H-Ta_2O_5 ss of composition $98Ta_2O_5$:$2Sc_2O_3$ were grown in the solid state using sealed or open Pt tubes at ≈1735°. The crystal structure of H-Ta_2O_5 stabilized by doping it with 2 mol% Sc_2O_3 and grown by the Czochralski technique has been reported.[1] Companion systems in the study of the stabilization of H-Ta_2O_5 are shown in Figs. 4340, 4347, 4363, 4400, 4410, 4413, 4425, 4449, and 4462–4464. Parallel studies in the stabilization of the low-temperature structure type are discussed with Fig. 4380.

1. N. C. Stephenson and R. S. Roth, *J. Solid State Chem.*, 3 [2] 145–53 (1971).

Sm_2O_3–HfO_2
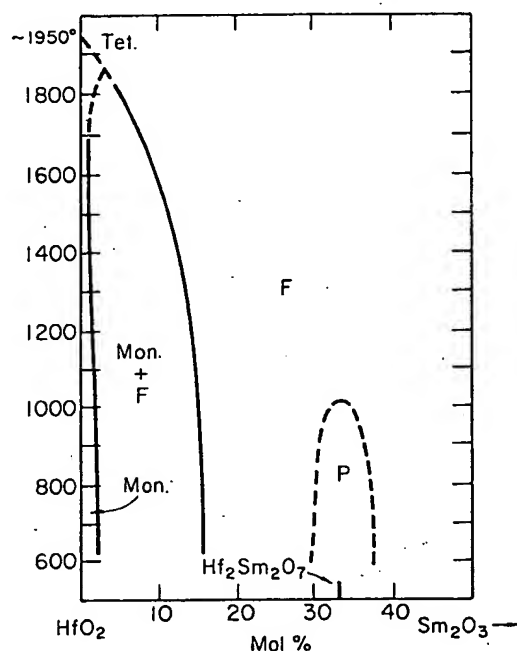
BEST AVAILABLE COPY

FIG. 4432.—System HfO_2–Sm_2O_3, subsolidus in HfO_2-rich region. Symmetry of phases: *F*, fluorite-type cubic; *Mon*, monoclinic; *Tet*, tetragonal; *P*, pyrochlore.

E. N. Isupova, V. B. Glushkova, and E. K. Keler, *Izv. Akad. Nauk SSSR, Neorg. Mater.*, 4 [3] 399 (1968); *Inorg. Mater. (USSR)*, 4 [3] 337 (1968).

Fourteen mixtures were prepared from 99.5 wt% HfO_2 and 99.8 wt% Sm_2O_3 by grinding, pressing, and firing at 1100° to 1600° in air in a Pt-Rh wound furnace and at 1700° in a W vacuum furnace. Thermal analysis to 1600° was conducted by DTA at a heating rate of 5°/min. X-ray diffraction analysis was done by the powder method, both on quenched specimens at room temperature and at high temperature in an X-ray furnace. Chemical analysis (for Sm and Hf) in the fired products was based on their selective solubility in HCl compared with the starting components.

Reaction of the components at 1200° proceeded at a low rate, and even at 1500° for 1.5 h the formation of equilibrium products was not complete. Prolonged heating at 1700° (8 to 10 h) was required to obtain a homogeneous single cubic fluorite-type solution. (Unit-cell length vs composition data are given.) Isothermal experiments at 1500° lasting 25 h established the mechanism of reaction between HfO_2 and Sm_2O_3. The primary reaction product formed was near the $Hf_2Sm_2O_7$ composition, and on continued heating this product reacted with the excess HfO_2 to form a solid solution of the starting composition.

As shown in the figure, the solubility of Sm_2O_3 in monoclinic HfO_2 decreases with a rise in temperature, from ≈2% at 1100° to 1% at 1700°. From analysis of high-temperature X-ray diffraction data, it was concluded that additions of Sm_2O_3 to HfO_2 lowered the monoclinic-to-tetragonal transition temperature (probably a second-order transition), but technical difficulties in photography at high temperatures precluded accurate quantitative measurements. Unit-cell dimensions for the tetragonal and monoclinic phases (containing 3% Sm_2O_3) are plotted as a function of temperature and indicate a decrease of ≈3% in molecular volume in the change to the high form. The transition from the ordered pyrochlore-type structure to the disordered fluorite structure takes place ≈1000° lower than in the Sm_2O_3–ZrO_2 system (Fig. 4433).

According to Ref. 1, HfO_2 shows 2 reversible transitions, i.e.

from monoclinic to tetragonal at 1900° to 2000° and from tetragonal to cubic at 2700°.

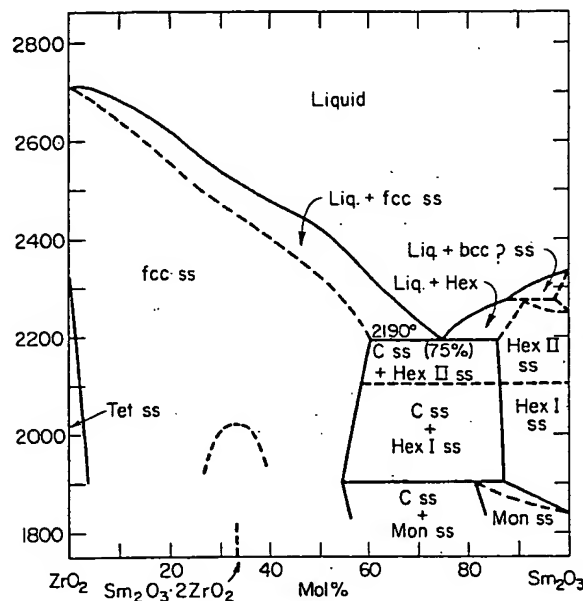1. A. G. Boganov, V. S. Rudenko, and L. P. Markov, *Dokl. Akad. Nauk SSSR*, 160 [5] 1065 (1965).

Sm_2O_3–ZrO_2

FIG. 4433.—System ZrO_2–Sm_2O_3 at high temperature; *bcc* = body-centered cubic, *fcc* = face-centered cubic, *Hex* = hexagonal, *Mon* = monoclinic, *Tet* = tetragonal, *C ss* = cubic solid solution, possibly *bcc*.

A. Rouanet and M. Foex, *C. R. Acad. Sci.*, *Ser. C*, 267 [15] 874 (1968).

The liquidus curve was derived from cooling curves obtained by the solidification of 23 compositions melted in a solar furnace. Phase transformations near 1900° in the region 65 to 95% Sm_2O_3 were observed at temperature by X-ray diffraction.

The diagram shows a number of discrepancies with previous data and must be considered provisional. It should be remembered, however, that the equipment for obtaining and measuring high temperatures accurately (> 1800°), as well as methods for identifying phases at high temperatures, is limited and generally unsatisfactory. The polymorphism of Sm_2O_3, e.g. the *Mon* → *Hex* I transition (corresponding to the rare earth *B* → *A* transition), the *Hex* I → II transition, and the high-temperature bcc form, does not agree with previous work (Figs. 2387 and 4255(*A*)). The high-temperature X-ray equipment was not considered sensitive enough to reveal superstructure lines at high temperature and at high concentrations of Sm_2O_3, which would distinguish the *C*-type (bcc) rare-earth oxide, identified at low temperatures, from the fcc ss.

A pyrochlore-type phase, $Sm_2O_3 \cdot 2ZrO_2$, with limited solid solution, was shown (by X-ray diffraction) as undergoing an order-disorder transformation at ≈2050° for the stoichiometric composition. This transformation is shown occurring at 2400° in Fig. 2387. The higher value is near the estimated solidus for the $Sm_2O_3 \cdot 2ZrO_2$ composition and would be more consistent with the inflection in the liquidus curve of Fig. 4433.

Figure 2387 resulted from a comprehensive study of ZrO_2 with the rare-earth oxides. Four types of furnace were used: for temperatures between 1300° and 1450°, a super Kanthal furnace; between 1450° and 1600°, a Pt-Rh-wound furnace; between 1600°

Y_2O_3-ZrO_2

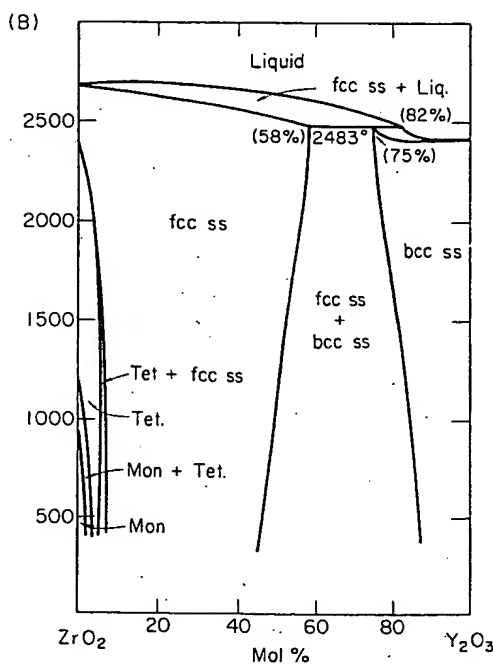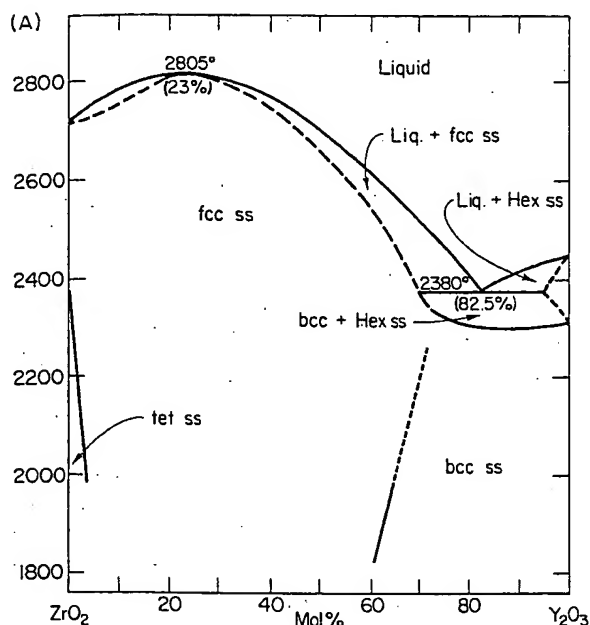
(A)
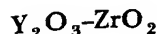
Fig. 4437.—System ZrO_2-Y_2O_3; *bcc* = body-centered cubic, *fcc* = face-centered cubic, *Hex* = hexagonal, *Tet* = tetragonal, *Mon* = monoclinic. (A) Above 2000°; A. Rouanet, C. R. *Acad. Sci.*, *Ser. C*, **267** [23] 1582 (1968). (B) Alternate composite diagram. Details of diagram for compositions containing <6.5% Y_2O_3 were taken from unpublished results of R. Ruh, K. S. Mazdiyasni, and K. O. Bielstein, *Amer. Ceram. Soc. Bull.*, **47** [4] 366 (1968) (abstract). S. R. Skaggs, Tech. Rept. SC–RR–72–0031, Jan. 1972; p. 89.

In Fig. 4437(A) 22 compositions, evenly distributed, were studied by thermal analysis for the determination of the liquidus and the solidus on the Y_2O_3-rich side. Seven compositions, all on the Y_2O_3-rich side, were studied by high-temperature X-ray diffraction to determine the subsolidus relations.

An interesting feature of this system is the continuous series of solid solutions varying from *fcc* on the ZrO_2-rich side to a *bcc* superstructure on the Y_2O_3-rich side. The line of demarcation is shown at that composition where the superstructure lines were first apparent by X-ray diffraction. A graph of cell size vs composition at room temperature is given for this series. There is some question as to the exact location of the subsolidus lines since they are inconsistent as shown.

In Fig. 4437(B) 20 compositions in 5 mol% intervals were prepared from > 99.7% ZrO_2 and > 99.9% Y_2O_3 powders by melting them in a CO_2 laser beam. A portion of the fused droplets was examined with an electron microprobe to determine actual chemical compositions and by X-ray diffraction to establish solid-state boundaries. Liquidus temperatures were determined from cooling curves obtained by remelting the other portions of fused samples. Temperatures, observed with an automatic optical pyrometer, were corrected using published emissivity values (0.84 for ZrO_2 and 0.96 for Y_2O_3).

Figure 4437(B) confirms the liquidus maximum shown in Fig. 4437(A) and reported by Noguchi[1] but indicates a solidus curve inconsistent with this finding. Moreover, Fig. 4437(B) omits the bcc-to-hexagonal transformation given in Fig. 4437(A) for Y_2O_3. Liquidus temperatures in Figs. 4437(A) and (B) differ in some regions by > 100° (e.g. a 2380° eutectic temperature in (A) vs a 2483° peritectic temperature in (B)), illustrating the difficulty of obtaining reliable measurements at extreme temperatures. A $Y_2Zr_2O_7$ compound postulated in Fig. 2390 was not found in the work represented by Figs. 4437(A) and (B).

The primary conflict appears to be the existence of a distinct 2-phase region (*fcc* ss + *bcc* ss) as shown in Figs. 4437(B) and 354. The structures of these phases are essentially the same (CaF_2 type), and evidence for 2 phases rests on the interpretation of X-ray diffraction data, i.e. the appearance of superstructure lines of Y_2O_3.

For similar studies on the ZrO_2-Er_2O_3 and ZrO_2-Yb_2O_3 systems, see Figs. 4405 and 4440. The polymorphism of ZrO_2 is discussed with Fig. 4259. However, in Fig. 4437(B) the monoclinic-to-tetragonal transformation is purposely drawn to indicate a large hysteresis, although the configuration does not obey the phase rule.

1. T. Noguchi, p. 249 in Advances in High Temperature Chemistry, Vol. 2. Edited by L. Eyring. Academic Press Inc., New York, 1969.

Y_2O_3–MoO_3
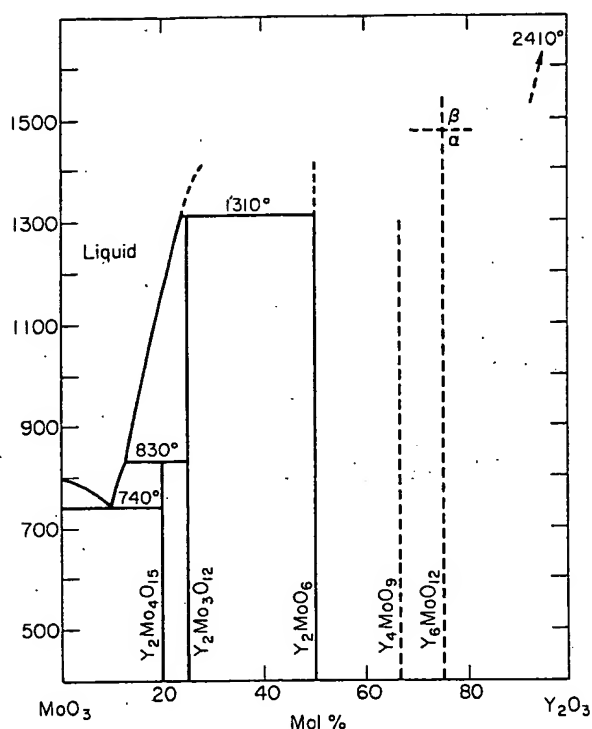
Fig. 4438.—System MoO_3–Y_2O_3 below 1500°.

J. P. Fournier, J. Fournier, and R. Kohlmuller, *Bull. Soc. Chim. Fr.*, 1970, No. 12, p. 4280.

MoO_3 (99% pure, Prolabo) and Y_2O_3 (> 99% pure) were formulated into mixtures by the solid-state method and studied by DTA and X-ray diffraction, as described with the companion system La_2O_3–MoO_3 (Fig. 4423).

Precautions must be observed with $Y_2Mo_3O_{12}$ because it hydrates in air to form $Y_2Mo_3O_{12} \cdot 4H_2O$. The experimental density and an unindexed X-ray powder pattern are listed for $Y_2Mo_3O_{12}$. Indexed patterns are given for Y_4MoO_9 and for α and β Y_6MoO_{12}.

Yb_2O_3–ThO_2
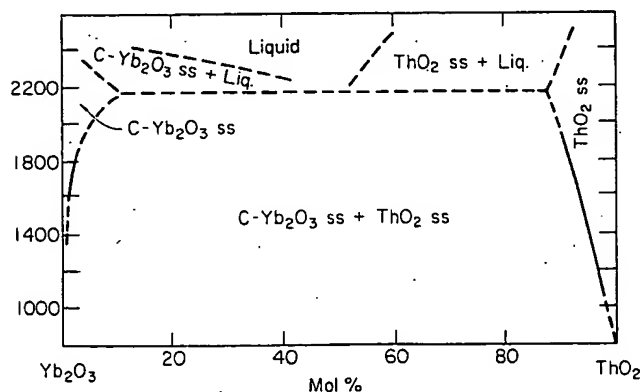
Fig. 4439.—System Yb_2O_3–ThO_2, tentative subsolidus.
A. M. Diness and R. Roy, *J. Mater. Sci.*, 4 [7] 618 (1969).

The materials and methods were the same as those described in the study of the companion systems La_2O_3–ThO_2 (Fig. 4420) and Gd_2O_3–ThO_2 (Fig. 4415). Visual observation of rounding and collapsing of particle aggregates on the heated Ir strip furnace was used to estimate liquidus temperatures and the position of the eutectic. As in the companion systems, various boundaries were located by plotting precision lattice parameters vs composition over a wide temperature range.

The solid-solubility limits at 1400° for Yb_2O_3 ss and ThO_2 ss are within experimental error of those reported by Gingerich and Brauer[1] in their study near 1400°. Point defects in the ThO_2 ss fluorite defect structure were characterized best by an anion-vacancy model.

1. K. A. Gingerich and G. Brauer, *Z. Anorg. Allg. Chem.*, 324 [1–2] 51 (1963).

Yb_2O_3–ZrO_2
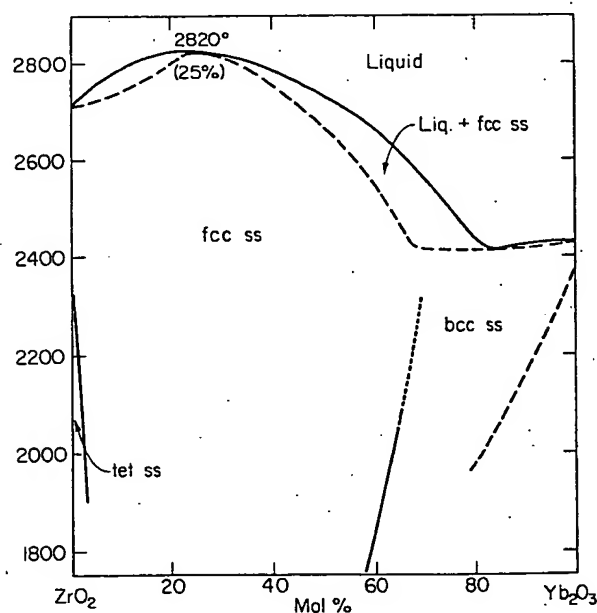
Fig. 4440.—System ZrO_2–Yb_2O_3 above 2000°; *bcc* = body-centered cubic, *fcc* = face-centered cubic, *tet* = tetragonal.
A. Rouanet, *C. R. Acad. Sci., Ser. C*, 267 [23] 1583 (1968).

Twenty-one compositions, evenly distributed, were studied by thermal analysis for the determination of the liquidus curve and the solidus on the Yb_2O_3-rich side. High-temperature X-ray diffraction was employed on 2 compositions to determine the line dividing the *fcc* and *bcc* areas.

An interesting feature of this system is the continuous series of solid solutions varying from *fcc* on the ZrO_2-rich side to a *bcc* superstructure on the Yb_2O_3-rich side. The line of demarcation is shown at that composition where the superstructure lines were first apparent by X-ray diffraction. A graph of cell size vs composition at room temperature is given for this series. The boundaries are in question because they are inconsistent as shown. The lower line on the Yb_2O_3 side marks a thermal effect thought by the investigator to result from dissociation of Yb_2O_3.

For similar studies on the systems ZrO_2–Er_2O_3 and ZrO_2–Y_2O_3, see Figs. 4405 and 4437. The polymorphism of ZrO_2 is discussed with Fig. 4259.

HfO$_2$–SiO$_2$ (concl.)

It is likely, in the opinion of the compilers, that this morphology was representative of cubic HfO$_2$, not detected in this work but reported at ≈2700° in Ref. 4 (see also Fig. 4444). The possibility of limited solubility of HfSiO$_4$ in HfO$_2$ was not explored.

1. C. E. Curtis, L. M. Doney, and J. B. Johnson, *J. Amer. Ceram. Soc.*, 37 [10] 458 (1954).
2. V. G. Chukhlantsev and Yu. M. Polezhaev, *Tr. Ural. Politekh. Inst.*, 1966, No. 148, p. 40.
3. D. J. Salt and G. Hornunf, *J. Amer. Ceram. Soc.*, 50 [10] 549 (1967).
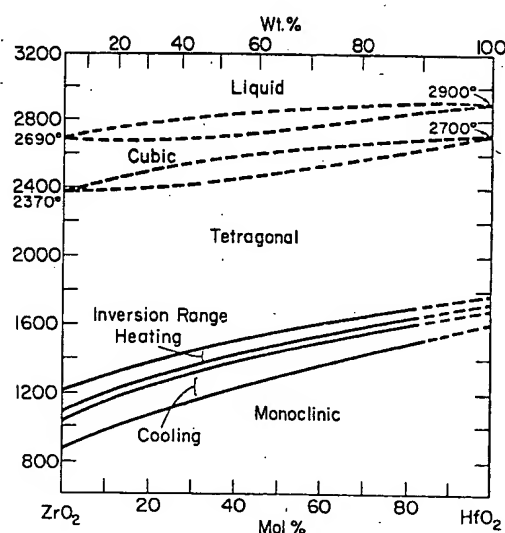4. A. G. Boganov, V. S. Rudenko, and L. P. Makarov, *Dokl. Akad. Nauk SSSR*, 160 [5] 1065 (1965).

HfO$_2$–ZrO$_2$

FIG. 4444.—System ZrO$_2$–HfO$_2$. The monoclinic ⇌ tetragonal inversion curves represent the start and finish of heating and cooling inversions, obtained by combining DTA and high-temperature X-ray data.

E. Ruh, H. J. Garrett, R. F. Domagala, and N. M. Tallan, *J. Amer. Ceram. Soc.*, 51 [1] 27 (1968).

Two sets of mixtures were made for this study, both from ZrO$_2$ reported to be 99.78% pure and reactor-grade HfO$_2$ (99.5% pure, including 2.2% ZrO$_2$). A few mixes were formulated with a spectrographic-grade HfO$_2$ (99.93%). The first group of 21 compositions, formulated at 5% intervals, was used for metallographic analysis, mp determination, room-temperature X-ray diffraction, and microprobe analysis. These were annealed and quenched from 800° to 1800° at 200° intervals. At 800°, treatments were conducted in evacuated fused-SiO$_2$ bulbs, and quenching was done in H$_2$O. At 1000° and 1200°, treatment was similar except that fused-SiO$_2$ bulbs with inert gas were used. At ≥ 1400°, treatment was conducted in a Pt-air furnace or a high-temperature vacuum resistance furnace. From the quench data for 1000°, a plot was made showing the continuous change in cell parameters of the monoclinic form vs composition from pure ZrO$_2$ to pure HfO$_2$. The mp's were determined in a special furnace[1] and are considered precise to ±30°. The mp's of ZrO$_2$ (2690°) and HfO$_2$ (2900°) were taken as base points to which the other data were corrected. Solid solutions require a solidus and liquidus temperature, but experimentally only a single (average) temperature was observed.

A second group of 10 samples, evenly distributed, was prepared for the DTA and high-temperature X-ray diffraction studies. These were made by grinding arc-melted compositions to −325 mesh, pressing them into wafers, and refiring the wafers to 2300° for 3 h in a vacuum-induction furnace.

The monoclinic-tetragonal and reverse inversions were determined by DTA in air using HfO$_2$ as the inert reference material. The inversion in all cases showed considerable hysteresis and did not seem time-dependent. High-temperature X-ray diffraction was also used to study the monoclinic-tetragonal and reverse inversions, using an induction-heated camera, with the sample on a W susceptor. The inversion of ZrO$_2$ covered a range of ≈137° on heating and ≈170° on cooling (see diagram). Temperature and reproducibility of the inversions were related to the thermal history and method of measurement and were found to be higher and with less range than reported by Wolten.[2]

The stable cubic phase shown on the diagram was not studied in this work. The diagram confirms the findings of Refs. 3 and 4 concerning a complete solid-solution series. The polymorphism of ZrO$_2$ is discussed for Fig. 4259.

1. R. F. Domagala and E. Heckenbach, *Rev. Sci. Instrum.*, 35 [12] 1663–64 (1964).
2. G. M. Wolten, *J. Amer. Ceram. Soc.*, 46 [9] 418–22 (1963).
3. C. E. Curtis, L. M. Doney, and J. R. Johnson, *ibid.*, 37 [10] 458–65 (1954).
4. O. M. Stansfield, *ibid.*, 48 [8] 436–37 (1965).

HfO$_2$–WO$_3$
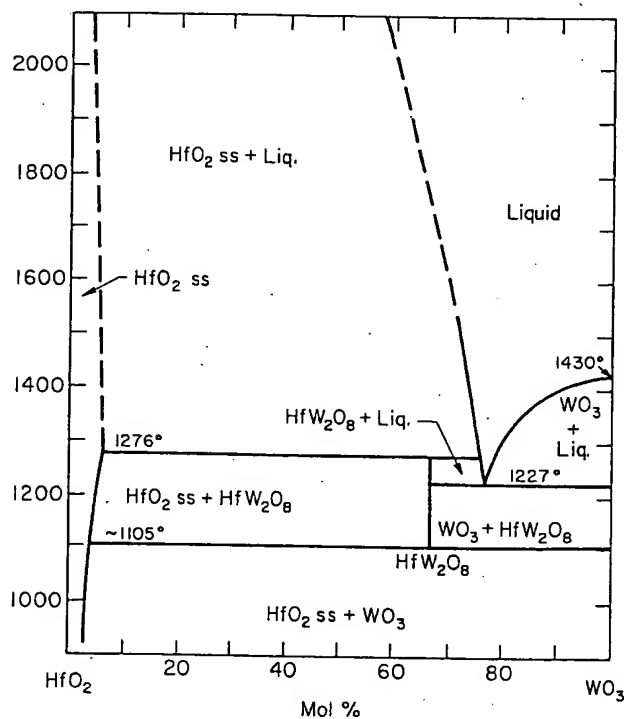
FIG. 4445.—System HfO$_2$–WO$_3$.

L. L. Y. Chang, M. G. Scroger, and B. Phillips, *J. Amer. Ceram. Soc.*, 50 [4] 213 (1967).

HfO$_2$ and tungstic anhydride, both purified (Fisher Scientific Co.), were used to prepare 14 samples, with special concentration between 60 and 80% WO$_3$. The methods, equipment, and results are similar to those described for Fig. 4459.

Fig. 4457   172   *Metal Oxide Systems*

BEST AVAILABLE COPY

UO₂–ZrO₂ (concl.)

above 1500° is after I. Cohen and B. E. Schaner, *J. Nucl. Mater.*, 9 [1] 33 (1963), modified by compilers to conform with the tetragonal-to-cubic inversion of ZrO_2 at 2372°. The region between 600° and 1200° and the extrapolation (dashed curve) to the boundaries of Cohen and Schaner are after K. A. Romberger, C. F. Baes, Jr., and H. H. Stone, *J. Inorg. Nucl. Chem.*, 29 [7] 1629 (1967). C = face-centered cubic ss, M = monoclinic ss, T = tetragonal ss.

The polymorphism of ZrO_2 is discussed with Fig. 4259. Pure UO_2 remains cubic up to its mp, which is listed for various conditions between 2176° and 2878° in Appendix I of the 1964 edition of Phase Diagrams for Ceramists. Lambertson and Mueller (reference cited) made an X-ray study of the system between 35 and 90% ZrO_2 using the quenching technique. Samples contained in W crucibles were heated in an He environment in a W-resistance furnace. The otherwise high-purity ZrO_2 (National Lead Co.) contained 2% HfO_2. To a greater or lesser extent, heated samples were contaminated with W. Unpublished data by Wisnyi[1] indicate that the solidus and liquidus curves are essentially coincident between ≈40 and 70 mol% ZrO_2. Below the liquidus, Lambertson and Mueller found a wide range of solid solution of the end-members, but their data are unreliable because of the failure to identify the nonquenchable cubic ZrO_2.

Cohen and Schaner (Fig. 2404) made a very careful study of the system above 1200° by X-ray and metallographic techniques. Their results showed a continuous face-centered cubic ss between 2300° and 2550°, confirming the existence of cubic ZrO_2. The materials used were natural micronized UO_2 powder prepared by reduction of UO_3 (Mallinckrodt Chemical Works) and ZrO_2 (containing 100 ppm maximum HfO_2) obtained from the Carborundum Co. The dry powders were blended, briquetted, and calcined at 1725° in H_2 to form UO_2–ZrO_2 solid solutions. The calcined briquets were crushed, ground, pressed into pellets, and sintered for 72 to 110 h at 1725° to 1750° in H_2. Most of the annealing was accomplished in an Mo-wound furnace at temperatures above 1200°, with flowing H_2 at 1 atm pressure. Temperatures were measured by a calibrated optical pyrometer under blackbody conditions. Annealed samples were quenched by pulling the Mo sample tray out of the hot zone. All samples were analyzed chemically for U and spectrochemically for major impurities after sintering. At lower temperatures, 14 compositions between 10 and 89.5 mol% ZrO_2 in 5 to 10% intervals, annealed as described, were studied at 10 temperatures between 1200° and 2100°.

Samples quenched from the high-temperature 2-phase region showed 2 phases, both identified as tetragonal by X-ray diffractometry. It was deduced, however, from metallographic techniques on NH_4F-etched platelets at ×200 to 1500 magnification that the equilibrium cubic phase transforms on cooling to a metastable tetragonal one characterized by an acicular or banded grain structure. A diffusionless transformation was found that extended from 55 mol% UO_2 to pure ZrO_2 in the region 1600° to ≈2285° (shown by dashed line in Fig. 2404). Contrary to previous reports (see superseded Figs. 119 and 120), a 2-phase field connecting the low-temperature miscibility gap with the cubic → tetragonal transformation of pure ZrO_2 was established.

Because of slow rates of reaction between the solid oxides below 1200°, Romberger et al. (reference cited) used a molten fluoride flux to speed the attainment of equilibrium at low temperatures. Starting materials consisted of $UO_{2.012}$ and ZrO_2 containing 99 ppm Hf. Three solid solutions of the oxides or their solid solutions (prepared by arc fusion) were equilibrated in an LiF–BeF₂–UF₄–ZrF₄ salt solution at various temperatures between 600° and 1130°. After filtration of the salt solutions, specimens were pulled from the furnace and air-cooled. Equilibration temperatures, measured with a calibrated Chromel-Alumel thermocouple, were controlled to within 1°. Petrographic examination showed that the specimens

contained both UO_2 and ZrO_2 solid-solution phases. The extent of mutual solid solubility between ZrO_2 and UO_2 was determined by analysis (colorimetric, spectrographic, and neutron activation) of chemically separated phases.

Romberger et al. revised Fig. 2404 below 1500° (dashed boundaries in Fig. 4456) for consistency with their low-temperature data, which indicated considerably less of the UO_2 and ZrO_2 solid solutions. The eutectic temperature was also located ≈1000° higher. These discrepancies cannot be adequately resolved without further research, especially on the effect of flux components. The use of a flux (of quaternary composition in this case) to study the binary system (now 6 components) must be viewed with the utmost caution. Consequently, the question regarding the extent of the low-temperature solid-solution boundaries has not been resolved.

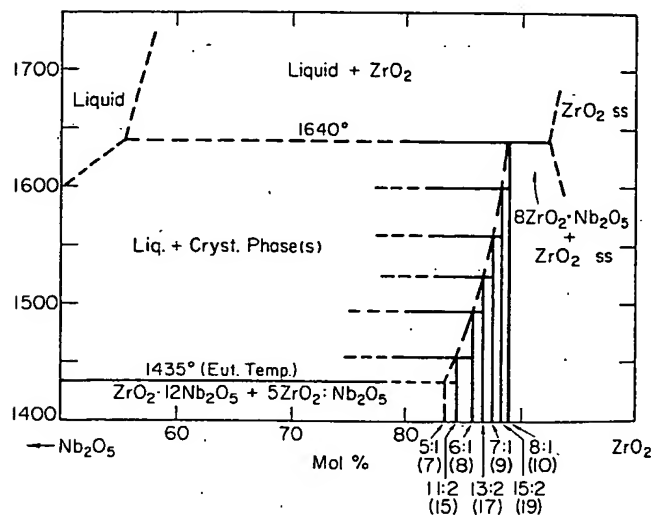1. L. G. Wisnyi, private communication; cited by Cohen and Schaner (reference cited).

ZrO₂–Nb₂O₅

FIG. 4457.—System Nb_2O_5–ZrO_2, proposed ZrO_2-rich portion, as modified by the compilers to conform with "Note Added in Proof." Numbers with colons indicate mole ratios of ZrO_2 to Nb_2O_5 of the proposed phases; numbers in parentheses indicate the multiplicity of the *b* axis of the proposed phases.

R. S. Roth, J. L. Waring, W. S. Brower, and H. S. Parker, *Nat. Bur. Stand. (U.S.), Spec. Publ.*, 1972, No. 364.

Twelve mixtures between 75 and 90% ZrO_2 and one at 50% ZrO_2 were prepared by the solid-state method of calcining pressed disks in air at 1000° for 10 h, cooling the material at 3°/min, re-pressing it into disks, and recalcining it at 1350° for 60 h, followed by cooling at 3°/min. Portions of these samples, contained in open Pt tubes, were studied by the quenching technique, with phase identification by X-ray diffractometry. To obtain unambiguous indexing of the powder patterns, small single crystals were grown either by slow cooling through the liquidus or by the addition of a eutectic flux (32.2 wt% BaO:67.8% V_2O_5) and heating of the mixtures to 1200° before slow cooling (1°/h) to 800°. The solidus temperature was easily detected by the appearance of low Nb_2O_5, which is the phase that recrystallizes from an Nb_2O_5-rich liquid on quenching.

In a note added in proof to the original manuscript, it is stated that the compositions were ≈0.5 to 1.5 mol% low in ZrO_2 because of nonreproducible weight losses of the starting ZrO_2 and that the correct compositions belonged to the homologous series $(Nb,Zr)_nO_{2n+2}$, not $(Nb,Zr)_{n-1}O_{2n}$. This change implied that the

ZrO_2–Nb_2O_5 (concl.)

phases were anion-excess fluorite type phases rather than cation deficient αPbO_2-type compounds. The conclusion was verified by Galy and Roth,[1] who determined the crystal structure of $Nb_2Zr_6O_{17}$ (6:1 in Fig. 4457). The specimens with more accurate mole ratios of Nb_2O_5 to ZrO_2 (1:5, 1:6, 1:7, and 1:8) were prepared by arc-fusion of pure end-member metals, which were then completely oxidized at 850° for 1 week, ground, and reheated at 1000° (with intermediate grinding) for another week.

Unlike the case for the Ta_2O_5–WO_3 system (Fig. 4466), the experimental evidence did not indicate a clear preference for discreet phases with discontinuous melting temperatures. It was concluded that 2-phase regions were unlikely to exist and that all compositions within the single phase were expressible by completely or almost completely ordered groupings of intermediate compositions and multiplicities. See Fig. 4466 for a discussion of the distinction between a single solid-solution phase and a series of phases in nonstoichiometric oxides.

This diagram differs from the corresponding region of Fig. 373 mainly in showing a narrower field of the orthorhombic phase(s) and in locating the composition of maximum stability at $8ZrO_2 \cdot Nb_2O_5$ rather than at $6ZrO_2 \cdot Nb_2O_5$. Indexed X-ray powder patterns are given for 6 compositions corresponding to the correct homologous series, $(Nb,Zr)_nO_{2n+2}$ (published compositions require adjustment, e.g. $Nb_4Zr_{15}O_{40}$ to $Nb_4Zr_{16}O_{42}$ and $Nb_4Zr_{10}O_{30}$ to $Nb_4Zr_{11}O_{32}$). The ZrO_2 ss region was not studied and is taken from Fig. 373. Figure 373 is in error, also, on the Nb_2O_5-rich side, since the compound $ZrO_2 \cdot 12Nb_2O_5$ is not shown. Allpress and Roth,[2] by combined X-ray diffraction and electron optical techniques, found the compound to exist in 3 polymorphs.

1. J. Galy and R. S. Roth, *J. Solid State Chem.*, 7 [3] 277 (1973).
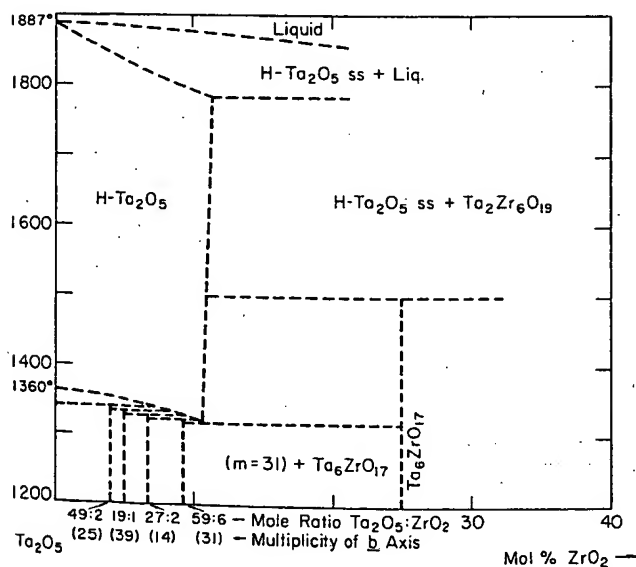2. J. G. Allpress and R. S. Roth, *J. Solid State Chem.*, 2 [3] 366 (1970).

ZrO_2–Ta_2O_5

Except for the following modifications, the materials, methods, and interpretation are similar to those for the companion Al_2O_3–

Ta_2O_5 system (Fig. 4380). Three compositions containing 5, 10, and 25% ZrO_2 (reagent grade) were prepared with the Ta_2O_5 by the solid-state method. Final heat treatments were done in sealed Pt tubes at temperatures between 1325° and 1590° for 4.5 to 19 h, before quenching and examination by X-ray diffraction powder techniques. It should be noted that the data may also be interpreted on the basis of a conventional solid-solution phase diagram, with a minimum in the solid-solution field. Figure 374 for the full system is obviously inadequate.
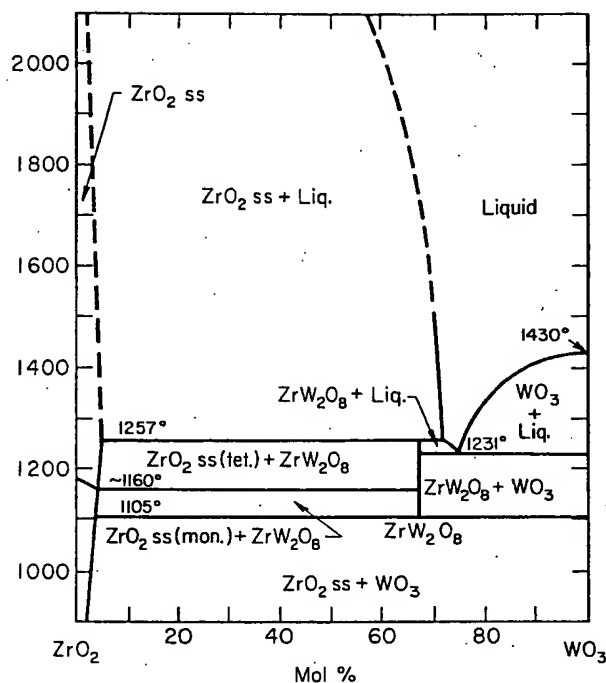
ZrO_2–WO_3

ZrO_2 and tungstic anhydride, both purified (Fisher Scientific Co.) were used to prepare 15 compositions, with special concentration between 65 and 80% WO_3. The mixtures were blended by tumbling for 2 h and then pelletized. The pellets were sealed in Pt tubes to prevent volatilization during heating. Quenches into water were made from an Mo-wound furnace above 1400° and from a Pt one below that temperature. Temperatures were controlled and measured to ±5° by a Pt–Pt10Rh thermocouple. DTA was employed to check melting relations and to determine nonquenchable phase transformations. Quenched samples were identified by reflected-light microscopy and by X-ray diffraction. The temperature of the monoclinic-tetragonal inversion of ZrO_2, as indicated by the beginning of the endothermal peak on the DTA heating curve, was almost 180° above the value cited in Ref. 1 (Fig. 355) but in agreement with Ref. 2. The compound ZrW_2O_8 was found, confirming Ref. 3. This compound can be obtained as a single phase only by heating the oxides in the proper ratio for at least 24 h near 1200°. The indexed powder pattern of ZrW_2O_8 is given.

1. P. Duwez and F. Odell, *J. Amer. Ceram. Soc.*, 33 [9] 280 (1950).
2. F. A. Mumpton and R. Roy, *ibid.*, 43 [5] 234–40 (1960).
3. J. Graham, A. D. Wadsley, J. H. Weymouth, and L. S. Williams, *ibid.*, 42 [11] 570 (1959).
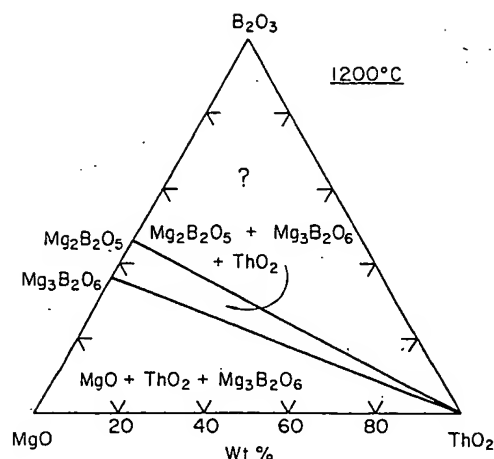
MgO–B$_2$O$_3$–ThO$_2$

FIG. 4571.—System MgO–ThO$_2$–B$_2$O$_3$, high-MgO corner at 1200°.

A. Whitaker and I. A. Darby, *J. Mater. Sci.*, 5 [12] 1088 (1970).

Fifteen compositions on or below the ThO$_2$–Mg$_2$B$_2$O$_5$ join were made from analytical-reagent-grade MgO, Th(NO$_3$)$_4$·6H$_2$O, and H$_3$BO$_3$, with respective purities not less than 99.2%, 99%, and 99.5%. Starting materials, except for H$_3$BO$_3$, were prefired (details given), mixed, pressed into pellets, heated on Pt foil at 1200° ± 5° for 4 h, and air-quenched. Three compacts containing only MgO and ThO$_2$ were heated for 26 to 28 h at 1200°. Eight of the compositions were analyzed chemically, and the average discrepancy was 0.8 wt%. Phases were identified by X-ray powder diffraction (Debye-Scherrer camera).

In the portion of the system studied, the presence of 2 binary compounds, Mg$_2$B$_2$O$_5$ and Mg$_3$B$_2$O$_6$, was confirmed (see Fig. 261). No intermediate phases or solid solutions were detected in the ternary mixtures or in the MgO–ThO$_2$ system, even after refiring at 1500° for 14 h in the latter case and the determination of accurate cell sizes by extrapolation against the Nelson-Riley function. In Fig. 722, however, ≈47 mol% (12 wt%) MgO is shown in solid solution with ThO$_2$ at 1600°. The limit of detectability of MgO in ThO$_2$ in the present work is estimated at ≈10 wt%. Therefore, if the disappearing-phase method had been used for Fig. 722, an erroneous solid-solution extent would have been obtained.
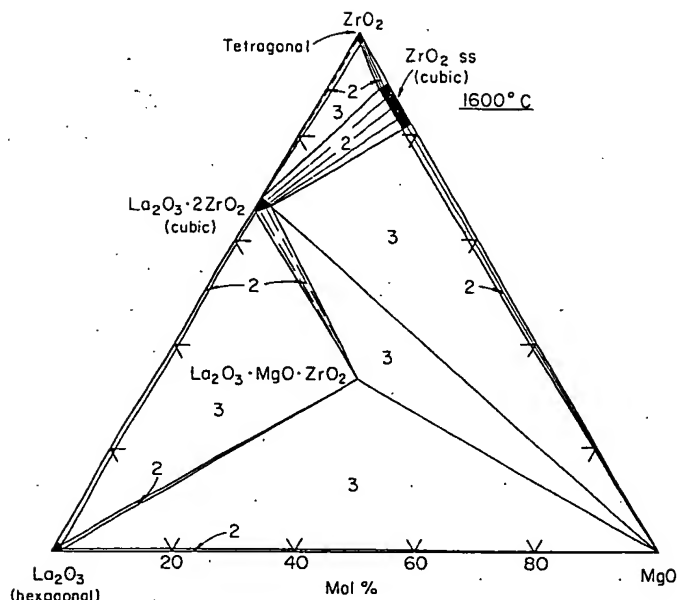
MgO–La$_2$O$_3$–ZrO$_2$

FIG. 4572.—System La$_2$O$_3$–MgO–ZrO$_2$, subsolidus at 1600° ± 20°. The numbers 2 and 3 refer, respectively, to 2- and 3-phase regions. Symmetry of the 4 solid-solution fields is indicated.

N. Schromek, *Ann. Chim. (Rome)*, 55 [1–2] 85 (1965).

Sixty-five compositions, with special concentration near the ZrO$_2$ corner and La$_2$O$_3$·2ZrO$_2$, were prepared from MgCO$_3$ (high-purity), La$_2$O$_3$ (BDH Laboratory), and ZrO$_2$ (TAM Div., National Lead Co.). Annealed samples were examined by X-ray analysis and by reflected-light microscopy. Photomicrographs typical of the various regions are shown and discussed.

Phase relations at 1400° were established on the basis of 17 compositions (table of data is presented but no diagram). The 1400° isotherm is similar to that at 1600°, except for a slight contraction of the tetragonal ZrO$_2$ ss field and a considerable decrease in the cubic ZrO$_2$ ss field. Below 1400° the cubic field tends to disappear. The 2 isotherms agree with Fig. 716 with respect to the ternary compound, but Fig. 716 shows a large "ZrO$_2$ cub. I" field instead of the correct La$_2$O$_3$·2ZrO$_2$ ss phase. Roth[1] reported this cubic pyrochlore-type compound.

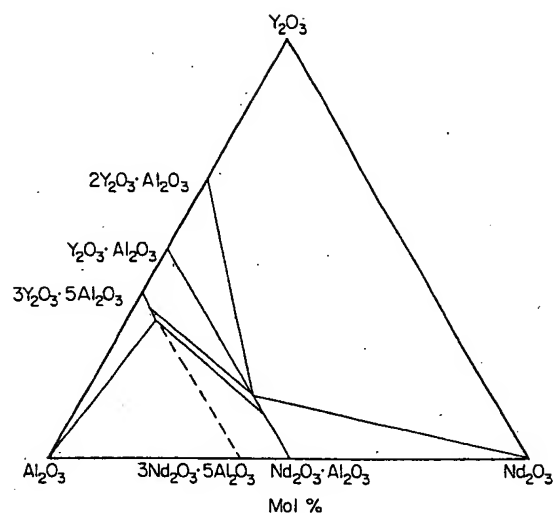1. R. S. Roth, *J. Res. Nat. Bur. Stand.*, 56 [1] 17 (1956).

Al_2O_3–Nd_2O_3–Y_2O_3

FIG. 4602.—System Al_2O_3–Nd_2O_3–Y_2O_3, subsolidus.
R. V. Bakradze, L. M. Kovba, G. P. Kuznetsova, and V. K. Trunov, *Dokl. Akad. Nauk SSSR*, **179** [4] 851 (1968); *Dokl. Chem.*, **179** [4] 279 (1968).

Because of experimental difficulties, samples were prepared by spontaneous crystallization from solution in a melt of PbO and PbF$_2$ to which was added B_2O_3. Starting materials were "pure"-grade Y_2O_3, PbF$_2$, and B_2O_3; N–2 grade Nd_2O_3; and analytical-grade Al_2O_3 and PbO. Samples were crystallized at a predetermined cooling schedule from a melt held at 1200°. Nd_2O_3 was introduced as $Nd_2O_3 \cdot Al_2O_3$ or $3Nd_2O_3 \cdot 5Al_2O_3$. Crystals were recovered from solidified material by heating it in dilute HNO$_3$. Compositions of the single crystals were established by optical crystallography, X-ray diffraction, and spectroscopic analysis.

Compositions of the single crystals were found to depend on the relative initial concentrations of Y_2O_3, Nd_2O_3, and Al_2O_3. The solubility of Nd in Y-Al garnet was a maximum ($\approx$12 wt%) along the section $3Y_2O_3 \cdot 5Al_2O_3$–"$3Nd_2O_3 \cdot 5Al_2O_3$." The relation of the lattice parameter to the composition of $(Y, Nd)_3Al_5O_{12}$ ss is shown. Because of the several fluxing agents used, the proposed phase diagram probably does not represent true ternary equilibrium.
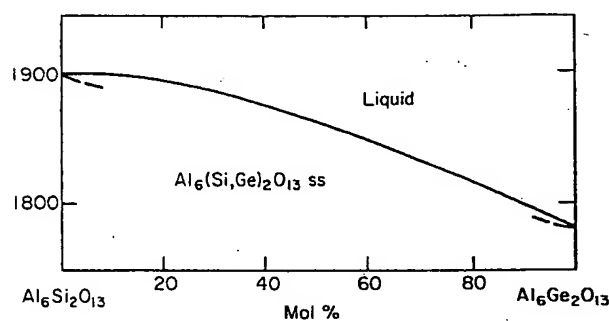
Al_2O_3–GeO_2–SiO_2

FIG. 4603.—System $Al_6Si_2O_{13}$–$Al_6Ge_2O_{13}$, liquidus.
N. A. Toropov, I. F. Andreev, V. A. Orlov, and S. P. Shmitt-Fogevlvich, *Izv. Akad. Nauk SSSR, Neorg. Mater.*, **6** [6] 1136 (1970); *Inorg. Mater. (USSR)*, **6** [6] 992 (1970).

Starting substances were γAl_2O_3 (obtained by heating NH$_4$-alum), SiO_2, and GeO_2 (specially-pure grade). A mixture corresponding to $Al_6Si_2O_{13}$ (mullite) was ground, pelletized, and heated at 1500° for 15 h with intermittent grinding every 5 h. $Al_6Ge_2O_{13}$ and 9 spaced intermediate mixtures of composition $Al_6(Si_xGe_{2-x})O_{13}$ were heated for 3 h each at 800°, 1000°, 1100°, 1250°, and 1350°. Chemical analysis showed that volatilization of GeO_2 was <1%. The stoichiometry was monitored also by weighing the specimens before and after each roasting. Melting points were determined in an electric microfurnace. Completeness of the synthesis was followed by chemical, microscopic, and X-ray powder diffraction methods.

The solidus curve was not defined, but from the nature of the liquidus it can be classified as Roozeboom type I (without maximum or minimum). Unit-cell constants (orthorhombic), refractive indices, densities, and molecular refractions are linear functions of the composition. Tables and plots of the data are given, including schematic X-ray diagrams and ir spectra of the solid solutions. The Al_2O_3–SiO_2 and Al_2O_3–GeO_2 diagrams, showing mullite formation, are found in Figs. 313, 314, and 4372.